Hindawi
Shock and Vibration
Volume 2019, Article ID 6830519, 13 pages
https://doi.org/10.1155/2019/6830519

Research Article

Stress Distribution and Fluctuation Cycle on the Rack Face of the Rock Cutting Tool

Xiaofeng Yang, Yongchao Xue, and Jiaheng Zhou

School of Mechanics and Civil Engineering, China University of Mining and Technology, Beijing 100083, China

Correspondence should be addressed to Xiaofeng Yang; act777@126.com

Received 8 August 2019; Revised 29 September 2019; Accepted 9 October 2019; Published 9 December 2019

Guest Editor: Franco Concli

The distribution of the stress field on the rack face has significant impacts on the performance and service life of the rock cutting tool. A dynamic simulation model of the stress on the rock cutting tool is established by finite element code Abaqus, and the distribution of local stress on the rack face and its impact factors are studied. It is concluded that the local stress on the rack face of the rock cutting tool shows obvious periodical fluctuation characteristics, and the fluctuation cycle of each point on the tool remains unchanged under the same cutting conditions. The stress fluctuation cycle period decreases with the increase of cutting speed inversely. The cutting depth and the back angle of the cutting tool have no obvious impact on the stress fluctuation period. However, the cutting depth and the back angle have obvious impacts on the average stress distributions of each point on the rack face of the tool. That is, the increase of back angle and cutting depth could cause the maximum stress point of the rack face to move upward to the tool tip.

1. Introduction

Rock drilling technology is widely used in mining, oil and gas development, and has more extended applications in the field of planet sampling, deep-sea, and geothermal engineering drilling recent years [1–5]. As the mechanism of cutting rock is very complicated, it is still difficult to estimate the stress of the tool accurately, though many researches on the theories of stress computation [6–12].

Experimental measures on the torque of PDC bit in rock drilling show that the variation of bit torque is consistent with the maximum lateral wear width of the bit [13]. Teale measured the cutting force of the rock wedge cutter at different angles, and the results show that the overall load of the cutter will increase when the wedge angle of the blade decreases, which would cause lower cutting stability [14]. Huang et al. measured and analyzed the overall cutting force of the tunnel boring machine; it shows that the overall cutting force of cutter head decreases with the increasing of mounting radius and linearly increases with the increasing of rotating speed [15]. However, due to the technology limitations of measurement methods, it is difficult to systematically reveal the relationship between the cutting parameters and the stress on the rock cutter.

Based on the establishment of numerical simulation of single-tooth rock cutting, Kuang et al. studied the relationship between cutting rake angle, side inclination angle, tooth diameter, and cutting depth and cutting force. The results are in good agreement with the experimental results [16]. Ouyang et al. investigated the rock cutting force by LS-DYNA simulation experiment. The results show that the cutting thickness, cutting angle, cutting width, and rock properties have significant impact on the cutting force [17]. Li et al. simulated and analyzed the overall stress of TBM cutter teeth during rock cutting using the finite element method. It is shown that the maximum cutting force varies constantly in motion and is closely related to the shear strength of rock [18]. Molecular dynamics simulation method is also adopted in the rock cutting process, and it is found that the friction force between the cutting tool and chip increases with the increasing of rake angle and cutting depth [19]. Meneze et al. found that the impact of cutting speed on the overall cutting force of the rock tool was not obvious through LS-DYNA simulation analysis [20]. The current of simulation research

mainly focuses on the overall force of the cutter, but there is little literature about the stress distribution characteristics in the rock cutting process. However, the local stress distribution on the cutter directly affects the failure type, damage position, and the service life of the tool. It is of great significance to research the distribution law of the stress on the rock cutting tool to study the mechanism of tool damage and improve the tool design [21–23].

In this paper, the rock cutting model of a nonrigid cutter is established based on the finite element method (FEM). Both distribution and fluctuation of the stress on the cutting surface of the rock cutting tool are studied, which would provide a persuasive reference for improving rock drilling efficiency and tool life.

2. Simulation Model and Parameters

2.1. Rock Damage Model and Cutting Separation Criteria. The Drucker–Prager model is used to describe the constitutive relationship of the rock. The yield criterion and plastic potential of the model can be expressed as [24–26]

$$\begin{aligned} f &= t - p\tan\beta - d = 0, \\ g &= t - p\tan\psi, \\ t &= \frac{q}{2}\left[1 + \frac{1}{k} - \left(1 - \frac{1}{k}\right)\left(\frac{r^3}{q}\right)\right], \end{aligned} \tag{1}$$

where t is the deviatoric stress, p is the equivalent compressive stress, β is the inclination angle of the linear yield surface, which is related to the friction angle φ of the material, g is the plastic potential function, ψ is the dilatancy angle, q is the Mises equivalent stress, k is the ratio of triaxial tensile strength to triaxial compression strength, r is the third invariant of deviatoric stress, and d is the cohesion of material.

The element failure in rock fracture process is mainly caused by both shear and compression effects. A plastic damage failure model is brought in to characterize the failure of elements (Figure 1). $\overline{\sigma}$ is the effective stress tensor without considering material damage, D is the damage variable, and E is the modulus of elasticity. σ_{y0} is the initial stress when the phenomenon of rock damage occurs. $\overline{\varepsilon}_0^{\mathrm{pl}}$ is the equivalent plastic strain corresponding to σ_{y0}. The relationship between stress tensor σ and D is defined by

$$\sigma = (1 - D)\overline{\sigma}. \tag{2}$$

The rock material is linear elastic until it reaches the yield stress σ_0. When the initial damage occurs in the rock, microcracks would appear in the interior of the rock. If the damage stress of the rock is exceeded, the material will soften due to internal microcracks, and $D = 0$ at this point. When the equivalent plastic strain of the rock σ_{y0} reaches the equivalent plastic strain of complete failure, $D = 1$. Also, the rock element will exfoliate from the rock mass without load and be deleted from the model [27–30]. Then, new elements continue to contact the tool and endure another period of elastic-plastic deformation and destruction.

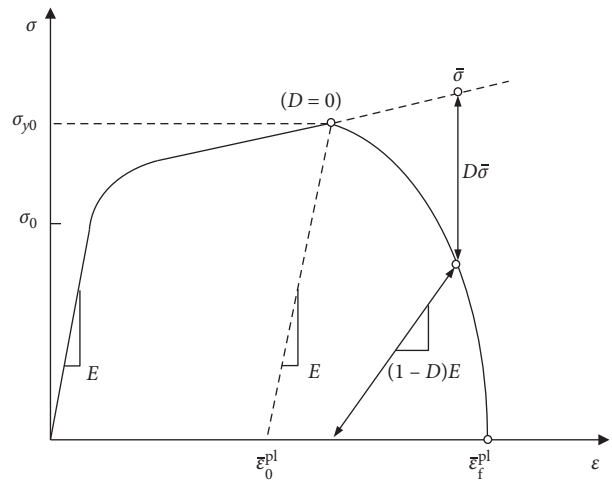

Figure 1: The plastic damage failure model.

2.2. Material and Model Parameters. The rock cutting simulations are performed by finite element code Abaqus. The rock material used in rock cutting simulation is sandstone, and the tool material is cemented carbide. The rake angle of the cutting tool is 10°. Material parameters are shown in Table 1.

The sandstone and cemented carbide are common homogeneous materials, and the tool and rock are set as isotropic materials in the model. Both the tool and the rock model are divided by quadrilateral grids. The size of the cutting tool is 40 mm × 70 mm, and a total of 900 grids are divided. The size of the cutting rock layer is 200 mm × 14 mm, which is divided into 7,000 refined grids. The size of the uncutting rock layer is 200 mm × 86 mm, which is divided into 2,500 grids. The computational grids of the simulation model remain unchanged with the cutting parameters. The surface-contact and self-contact are adopted for defining of contact attributes.

To study the dynamic patterns of the stress on the cutter, the tool is set as nonrigid body, and the variation of stress on each point of the rock cutting tool is discussed under different cutting parameters. The cutting parameters of cutting speed, cutting depth, and the back angle of the cutting tool are shown in Table 2.

Both the rock and the tool are axisymmetric structures, and the cutting is conducted in one-dimensional horizontal direction, so two-dimensional simulation analysis model is performed to improve the calculation efficiency (Figure 2).

3. Results and Discussion

3.1. Cutting Tool Stress Distribution. Figure 3 shows the stress distribution of the cutting tool when the back angle of the tool is 10°, the cutting depth is 10 mm, and the cutting speed is 1.36 m/s. A concentration of stress occurs at the tool tip immediately when the cutting starts. Then, the tip stress decreases but the stress of other positions increases and spreads to both sides along the front and back tool surface like a parabola. A stress concentration area is formed on the

Table 1: Rock and tool material parameters.

Materials	Elasticity modulus (GPa)	Density ($kg \cdot m^{-3}$)	Poisson ratio	Internal friction angle (°)	Cohesion (MPa)	Compressive strength (MPa)	Dilation angle (°)	Fracture strain
Sandstone	5.6	2500	0.168	24.47	26.13	67.2	20.3	0.0067
Cemented carbide	800	15000	0.2	—	—	—	—	—

Table 2: Cutting parameters.

Working condition	Variable
Back angle(°) (α)	5/10/15/20
Cutting depth(mm) (H)	8/10/12/14
Cutting speed ($m \cdot s^{-1}$) (V)	0.46/0.65/0.92/1.36/1.90

front and back of the tool near the tip, forming a triangular risk region. The stress of each element on the cutter stabilizes within a certain range after about 1.75 ms.

It is also shown that the stress concentration is higher on the rack face (Figure 3). In order to better observe the specific distribution of stress, the rack face is divided into 30 elements, whose mesh deviation ratio is 10. The first 10 elements are numbered 1–10# in turn from the tip on the rack face (Figure 4) so that the stress variation of each element could be calculated and analyzed, respectively.

3.2. Characteristics of Stress Fluctuation on the Rack Face

3.2.1. Stress Distribution on the Rack Face. The stress-time curves (Figure 5) show that the stress changing can be divided into two stages. At the beginning of cutting (0-1 ms), the impact stress of each element zooms obviously. Then, the stress falls and enters into a stable cutting stage (>1 ms) and fluctuates within a certain range. Figure 5 also shows that the average stress of the element at different positions is different.

Figure 6 shows the magnification curve of stress fluctuation with the sampling interval of 0.233 ms. It is shown that the stress distribution of each element has an obvious periodical fluctuation, and each element will have a fluctuation cycle of $T = 5t = 0.233\ \text{ms} \times 5 = 1.17\ \text{ms}$.

It is found that the stress fluctuation of each element also has periodic patterns under different tool back angles and cutting speeds (Figures 7 and 8). The stress fluctuation period of each point on the tool rack face appears to be the same under the same cutting parameters. However, the changing of the cutting parameters may affect the fluctuation period.

3.2.2. The Influence of Tool Back Angle on Stress Fluctuation. The cutting speed is set at 1.36 m/s, the cutting depth is 10 mm, and the influence of the back angle on the stress fluctuation period is observed at 5°, 10°, 15°, and 20°, respectively. No.1 element is taken as an analysis example for its stable rock-tool interaction. Figure 9 indicates that the back angle of the cutting tool has no obvious influence on the stress fluctuation period ($T = 5t$).

3.2.3. Influence of Cutting Depth on Tool Stress Fluctuation. The cutting speed is set at 1.36 m/s, the cutting angle is 10°, and the influence of cutting depth on the stress fluctuation period is observed at 8 mm, 10 mm, 12 mm, and 14 mm, respectively. Figure 10 shows that the stress on the rack face presents periodic fluctuation under different cutting depths with the same periods $T = 5t$, indicating that the cutting depth has no significant influence on the stress fluctuation period.

3.2.4. The Influence of Cutting Speed on Stress Fluctuation. The cutting angle is set at 10°, the cutting depth at 10 mm, and the influence of the cutting speed on the stress fluctuation period is observed at 0.46 m/s, 0.65 m/s, 0.92 m/s, 1.36 m/s, and 1.9 m/s, respectively.

Figure 11 shows that the cutting speed has a significant impact on the stress fluctuation period. The stress fluctuation period decreases with the increase of the cutting speed.

Figure 12 shows the fitting curve graph which reveals the relationship between stress fluctuation period and cutting speed. It is shown that the stress fluctuation period is inversely proportional to the cutting speed ($T = 9.25v^{-1}$).

The stress in the microscopic areas of the rack face is mainly affected by the specific interaction between the rock particles and the tool. The microcutting debris would impact the tool rack face continuously in the rock cutting. However, the higher cutting speed will increase the impact frequency of debris particles on the rack face, leading to a lower stress fluctuation period (Figure 13).

3.3. Average Stress on the Rack Face

3.3.1. The Influence of the Back Angle Cutting Tool on Average Stress. The influence of cutting parameters on the average stress of each element on the rack face is studied. The cutting speed is set at 1.36 m/s, the cutting depth is 10 mm, and the influence of the back angle on the average stress is observed at 5°, 10°, 15°, and 20°, respectively.

It is shown that the stress of each element changes linearly along the tool tip under different back angles (Figure 14). The increase of the back angle could cause the maximum stress point to move upward from the tool tip to the top along the rack face. Besides, the larger back angle induces greater average stress to each element.

The tool stress is closely related to the deformation. The larger the tool back angle, the smaller the wedge angle of the tip and the greater the deformation of the tool (Figure 15), causing the increase of the average stress and the maximum stress position to move upward to the top (Figure 16). It means that the larger the back angle of the tool is, the more

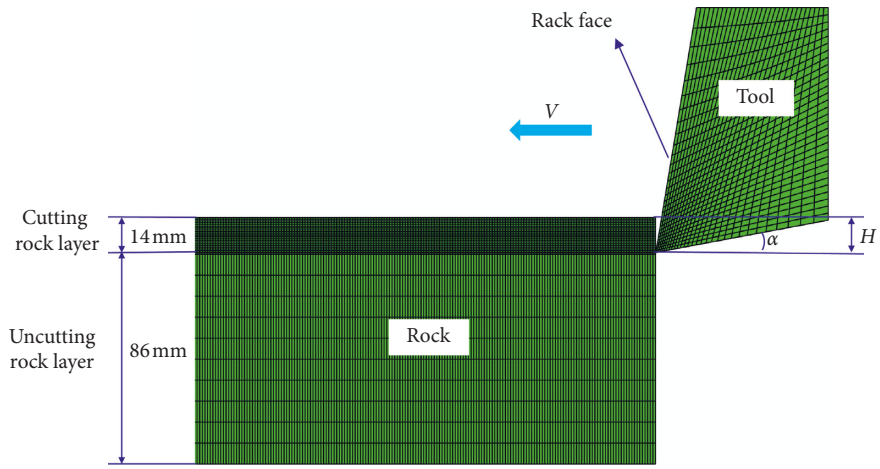

FIGURE 2: Schematic simulation model of the rock cutting (back angle $\alpha = 5$–20°, cutting depth $H = 8$–14 mm, and cutting speed $V = 0.46$–1.90 m/s).

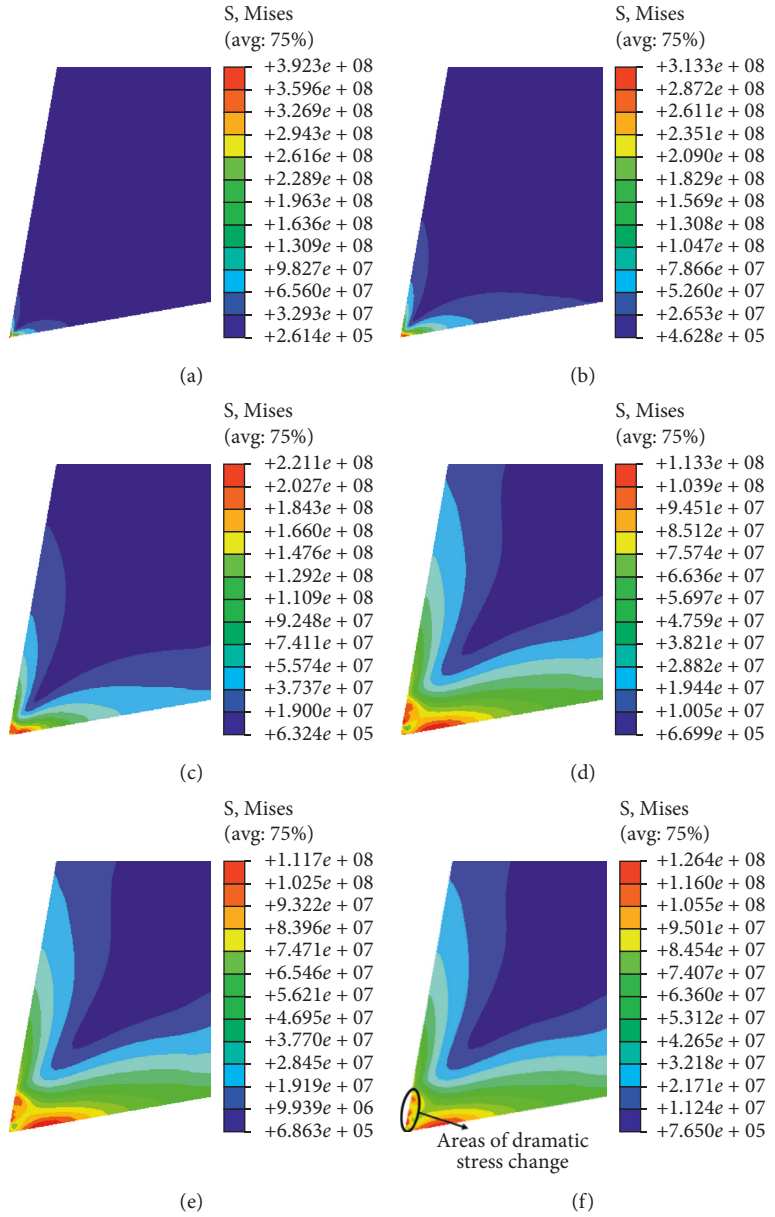

FIGURE 3: Stress distribution on the cutting tool (α=10°, $H = 10$ mm, and $V = 1.36$ m/s): (a) $t = 0.35$ ms; (b) $t = 0.7$ ms; (c) $t = 1.05$ ms; (d) $t = 1.75$ ms; (e) $t = 35$ ms; (f) $t = 70$ ms.

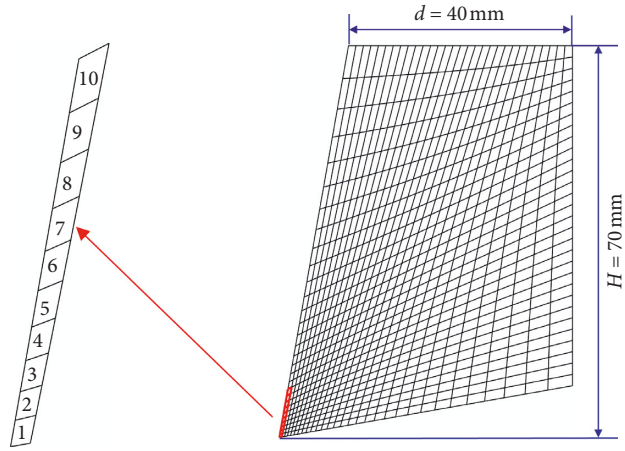

Figure 4: Schematic diagram of main contact elements on the rack face.

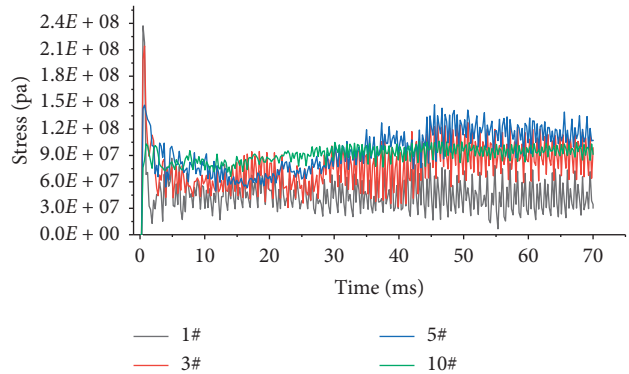

Figure 5: Stress-time curves of the representative elements on the rack face ($\alpha = 10^{\circ}$, $H = 10$ mm, and $V = 1.36$ m/s).

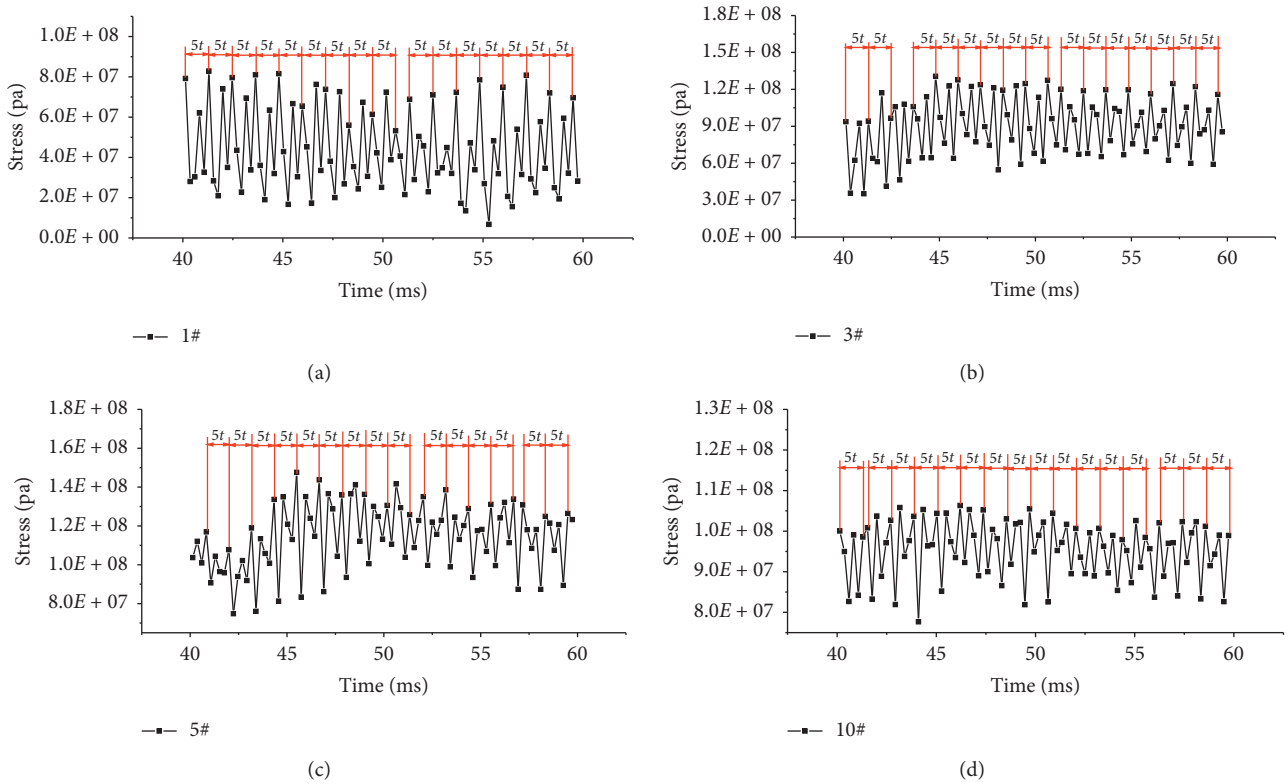

Figure 6: Stress fluctuation cycle period of the representative elements ($\alpha = 10^{\circ}$, $H = 10$ mm, and $V = 1.36$ m/s): (a) 1# element; (b) 3# element; (c) 5# element; (d) 10# element.

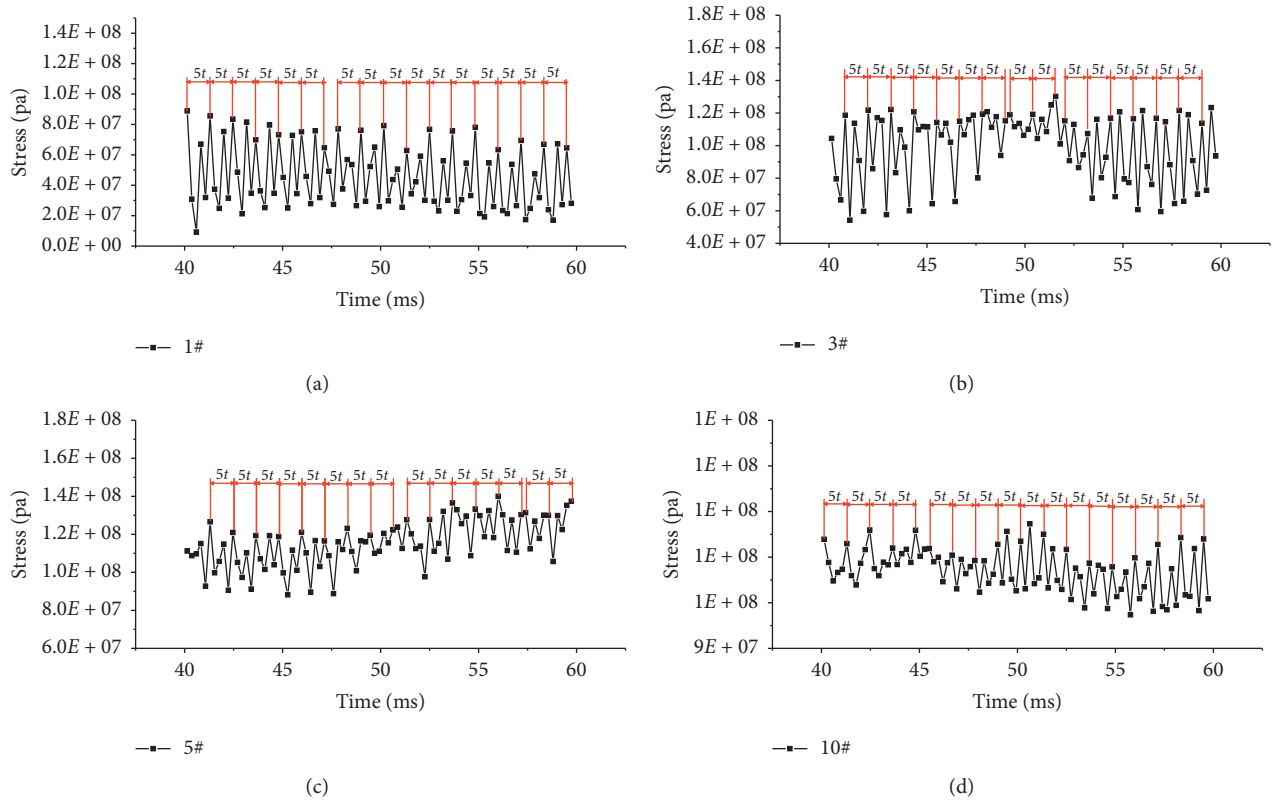

Figure 7: Stress fluctuation cycle period of the representative elements ($\alpha = 20^{\circ}$, $H = 10$ mm, and $V = 1.36$ m/s): (a) 1# element; (b) 3# element; (c) 5# element; (d) 10# element.

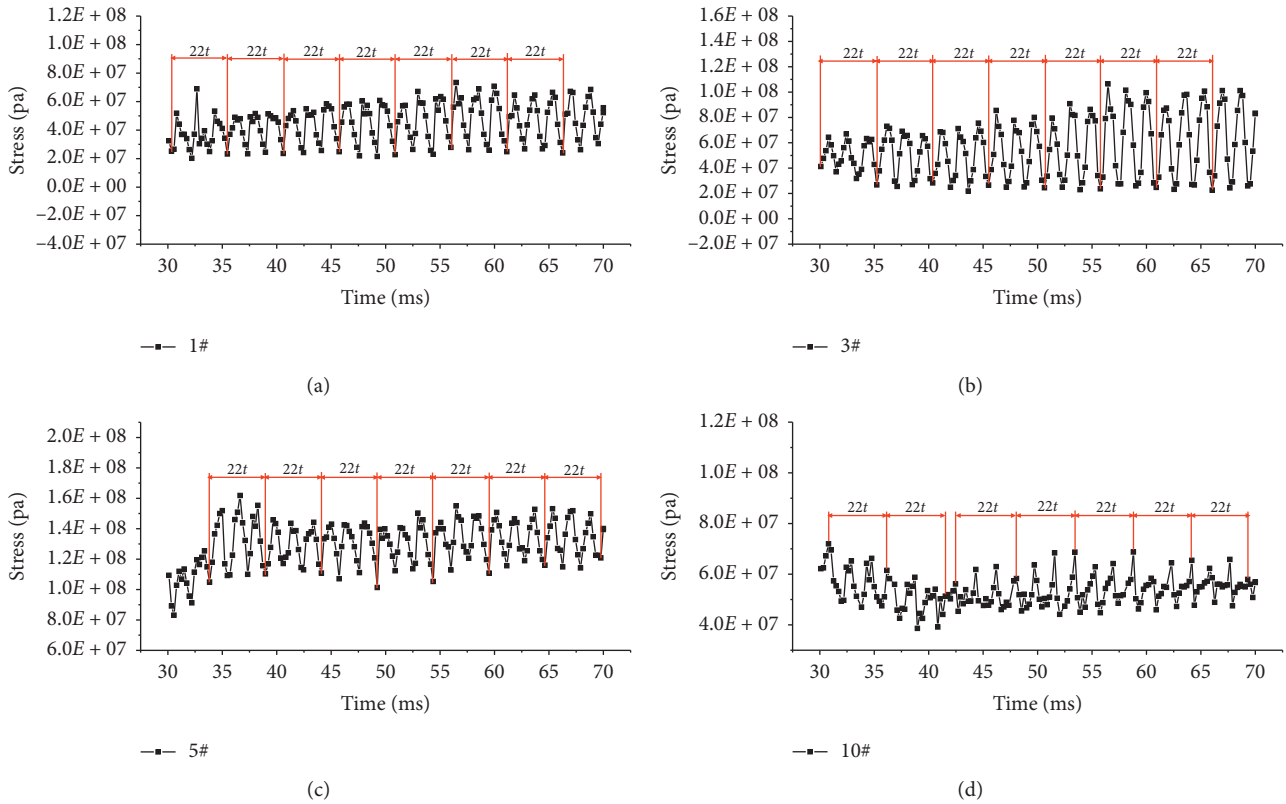

Figure 8: Stress fluctuation cycle period of the representative elements ($\alpha = 10^{\circ}$, $H = 10$ mm, and $V = 0.46$ m/s): (a) 1# element; (b) 3# element; (c) 5# element; (d) 10# element.

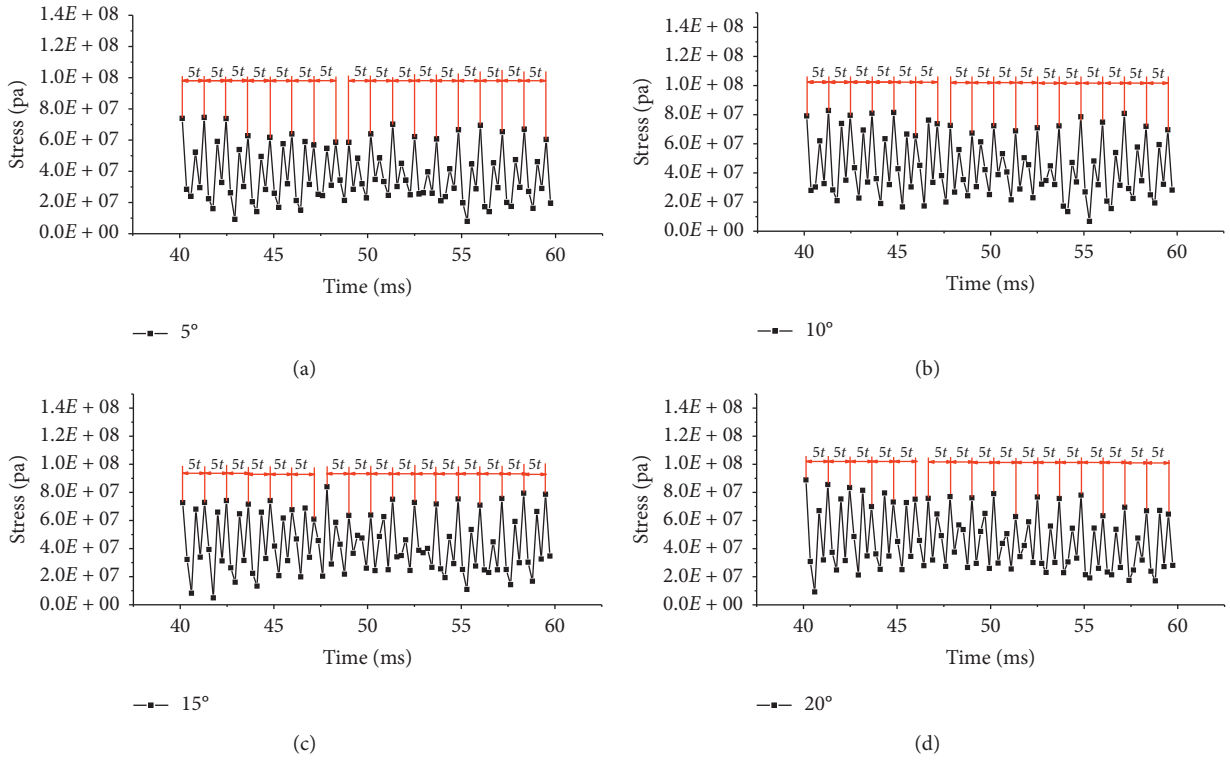

Figure 9: Stress fluctuation cycle period under different tool back angles ($H = 10$ mm and $V = 1.36$ m/s): (a) $\alpha = 5^{\circ}$; (b) $\alpha = 10^{\circ}$; (c) $\alpha = 15^{\circ}$; (d) $\alpha = 20^{\circ}$.

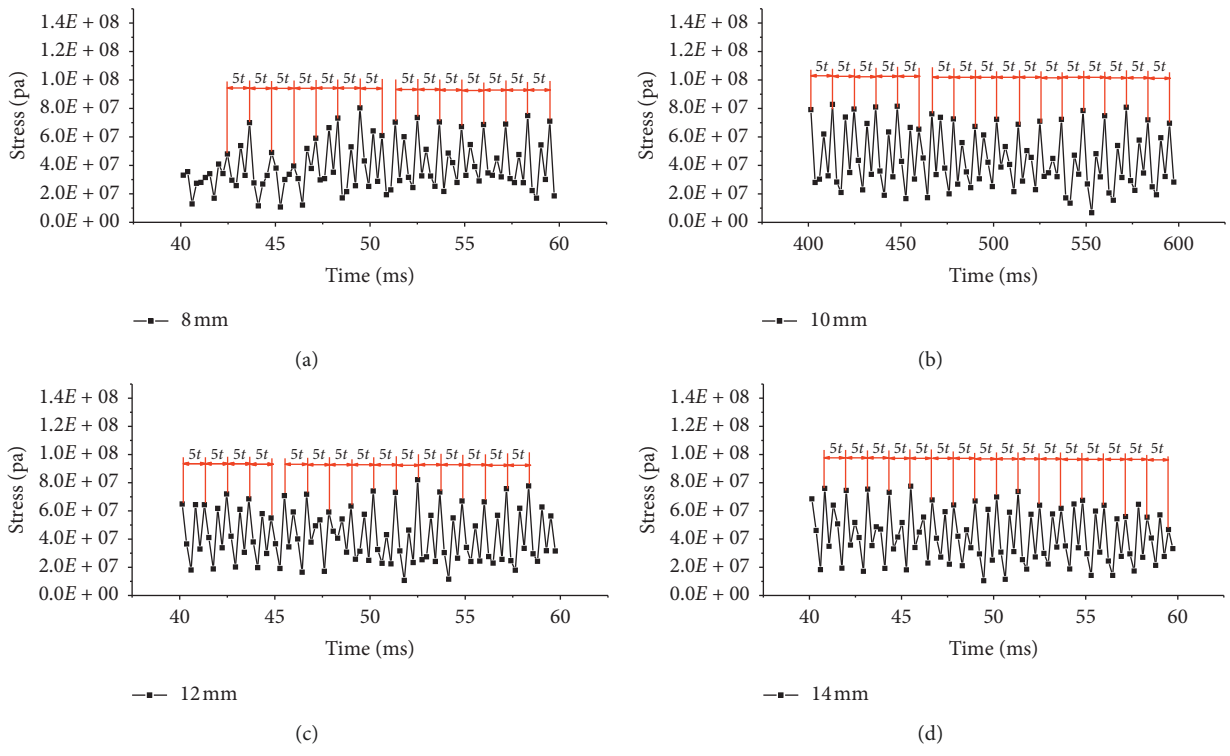

Figure 10: Stress fluctuation cycle period at different cutting depths (α=10° and $V = 1.36$ m/s): (a) $h = 8$ mm; (b) $h = 10$ mm; (c) $h = 12$ mm; (d) $h = 14$ mm.

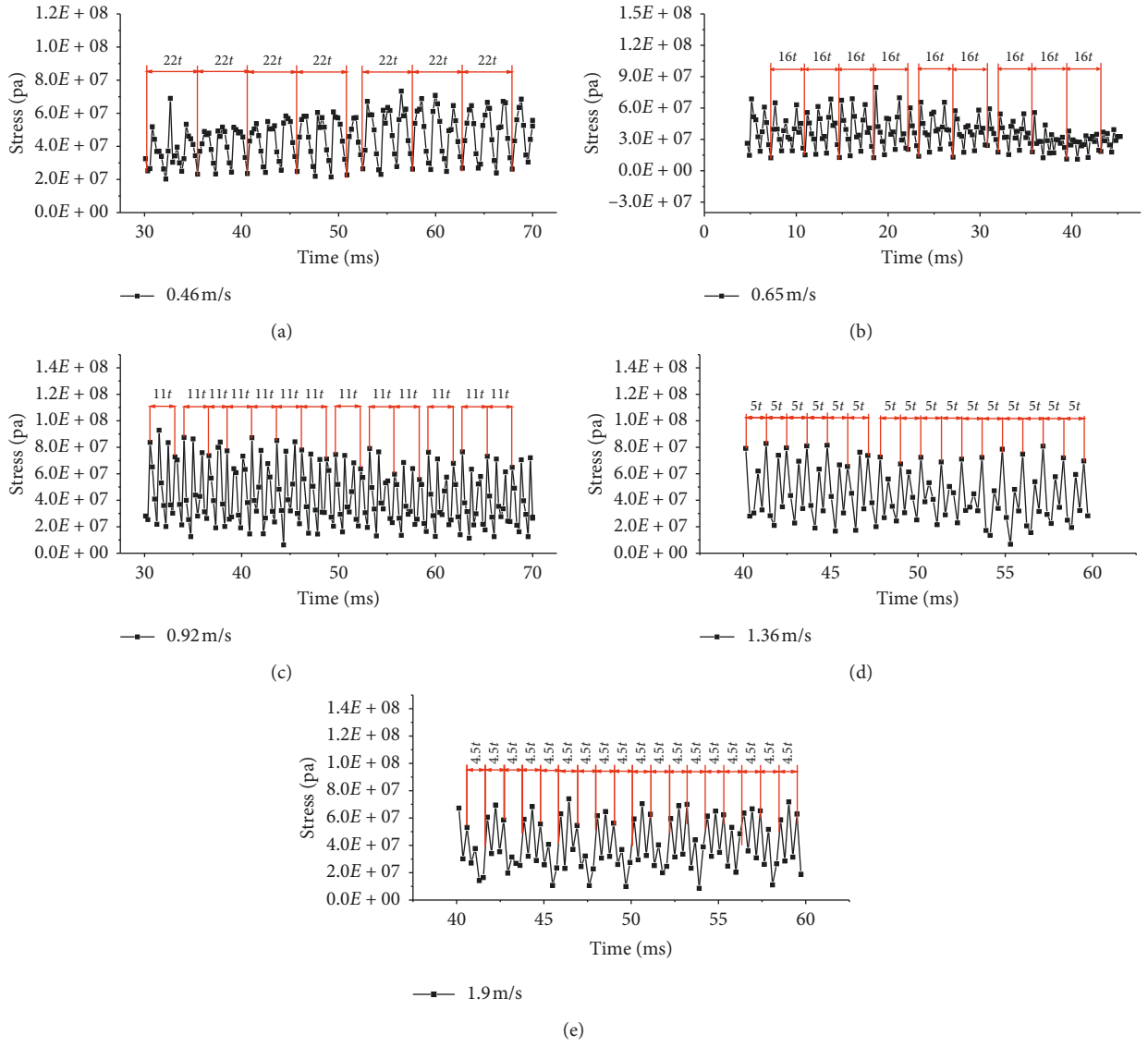

Figure 11: Stress fluctuation cycle period at different cutting speeds ($\alpha = 10^{\circ}$ and $H = 10$ mm): (a) $v = 0.46$ m/s; (b) $v = 0.65$ m/s; (c) $v = 0.92$ m/s; (d) $v = 1.36$ m/s; (e) $v = 1.36$ m/s.

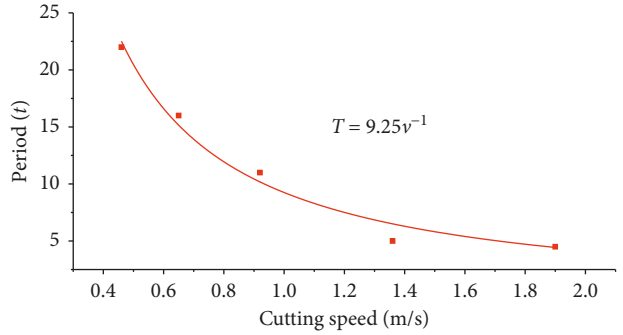

Figure 12: The influence of cutting speed on the stress fluctuation cycle period ($\alpha = 10^{\circ}$ and $H = 10$ mm).

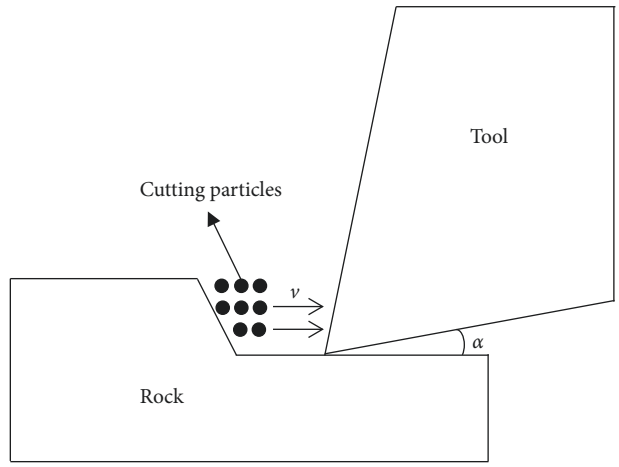

Figure 13: Schematic of the impacts of the cutting particles on the rack face.

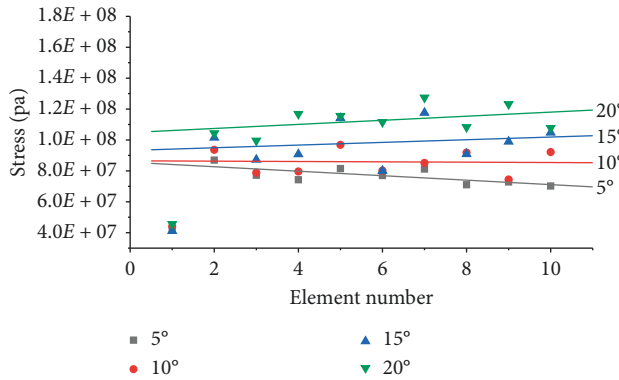

Figure 14: The average stress of representative elements under different tool back angles ($H = 10$ mm and $V = 1.36$ mm/s).

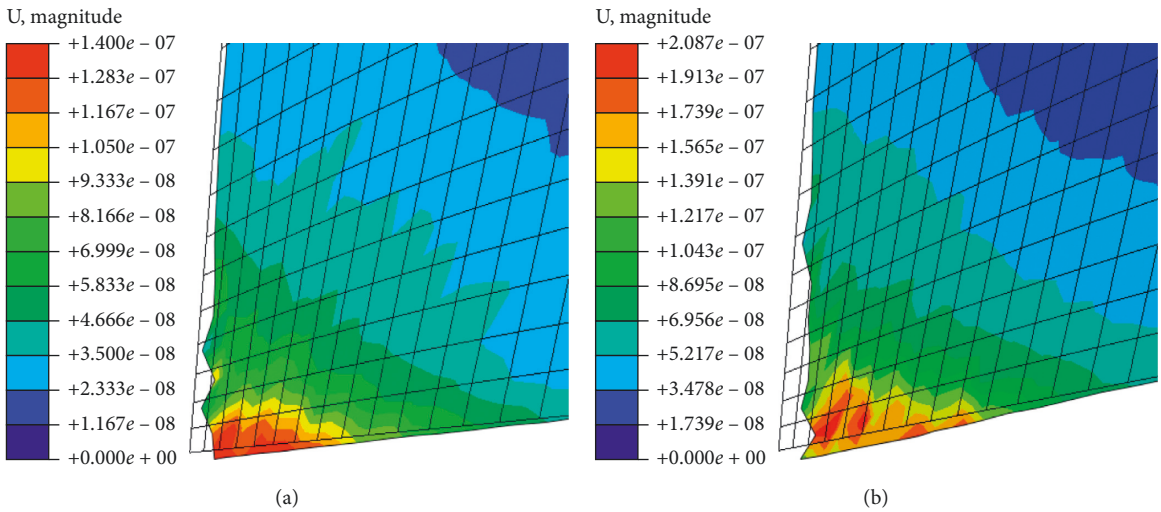

Figure 15: Continued.

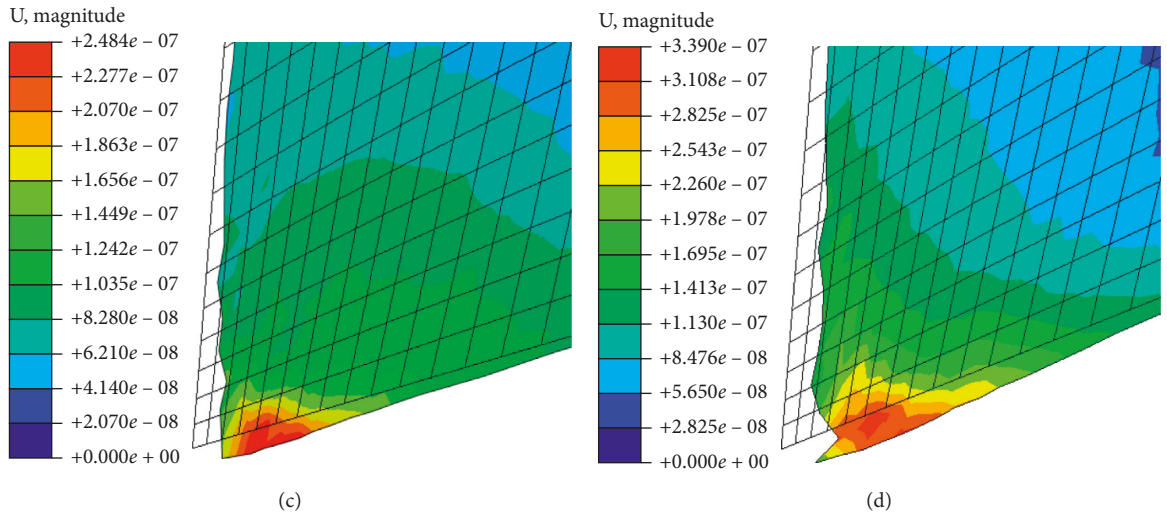

FIGURE 15: The amplified deformation of the tool under different tool back angles ($H = 10$ mm and $V = 1.36$ m/s): (a) $\alpha = 5^{\circ}$; (b) $\alpha = 10^{\circ}$; (c) $\alpha = 15^{\circ}$; (d) $\alpha = 20^{\circ}$.

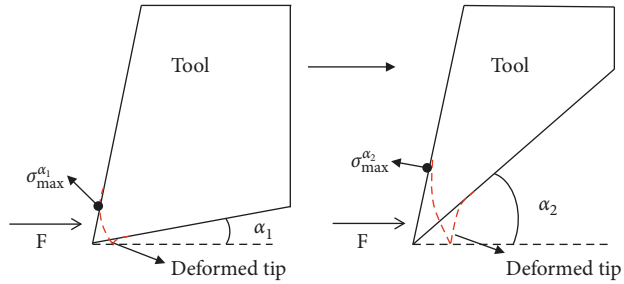

FIGURE 16: Schematic of deformation and stress on the rack face under different tool back angles.

likely the tool rack face would be damaged and the vulnerable point would rise along the rack face.

3.3.2. The Influence of Cutting Depth on Average Stress. The cutting speed is set at 1.36 m/s, the back angle is 10°, and the influence of the cutting depth on the average stress is observed at 8 mm, 10 mm, 12 mm, and 14 mm, respectively. Figure 17 shows that the stress of each element changes linearly along the tool tip under different cutting depths. As the cutting depth steadily increases, the maximum stress point moves upwards from the tool tip to the top along the rack face.

There is a dense core of chip particles in front of the rack face in rock cutting [9]. With the increase of cutting depth, the volume of the dense core enlarges and the center of the dense core moves upwards to the top, which leads to the rise of the maximum stress point along the tool rack face (Figure 18). It means that the vulnerable position would move upwards from the tool tip to the top along the rack face. This conclusion is basically consistent with the experimental results of relevant literature (Figure 19) [29].

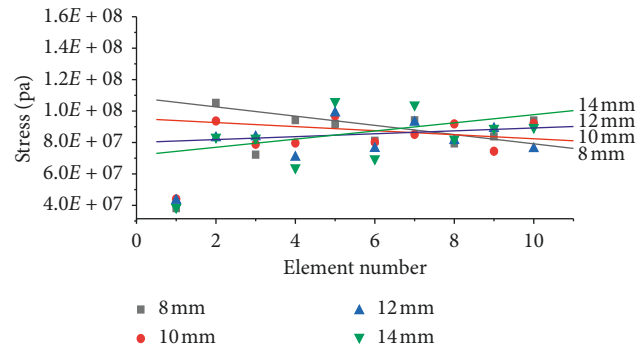

FIGURE 17: The average stress of representative elements under different cutting depths ($\alpha = 10^{\circ}$ and $V = 1.36$ mm/s).

3.3.3. The Influence of Cutting Speed on Average Stress. The cutting depth is set at 10 mm, the back angle is 10°, and the influence of the cutting speed on the average stress is observed at 0.46 m/s, 0.65 m/s, 0.92 m/s, and 1.36 m/s, respectively. Although the average stress of each element on the rack face fluctuates slightly, the stress fitting curves are almost at the same level under different cutting speeds

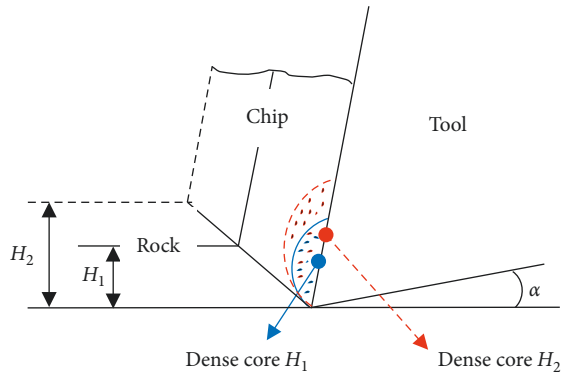

Figure 18: Schematic of the maximum stress point on the rack face.

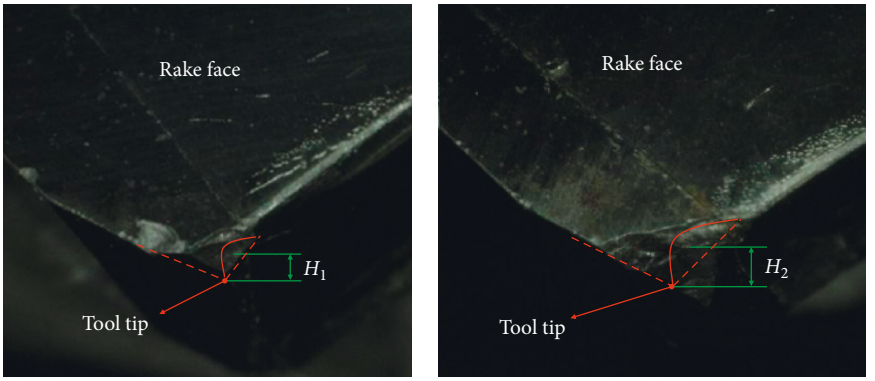

(a) (b)

Figure 19: Tool damage under different cutting depths (adapted from ref. [29]). (a) Smaller cutting depth. (b) Larger cutting depth.

(Figure 20). This indicates that the cutting speed has no obvious influence on the average stress of each element.

4. Conclusion

A dynamic simulation model of the tool stress in rock cutting process is established. The distribution of local stress on the rack face and its influencing factors were studied. Based on the research presented in this paper, the following conclusions could be drawn:

(1) The stress concentration on the rack face is higher than that on the back surface. After working about 17.5 ms, the stress at each position of the tool reaches the maximum value and fluctuates steadily within a certain range. A risk region of stress concentration is formed at the tip of the tool.

(2) The stress fluctuation of each point on the rack face of the rock cutting tool shows obvious periodic characteristics, and the stress fluctuation cycle of each point on the rack face is the same under the same cutting conditions. The stress fluctuation cycle period decreases with the increase of cutting speed under a reverse proportional tendency. The cutting depth and the back angle of the cutting tool have no obvious impact on the stress fluctuation period.

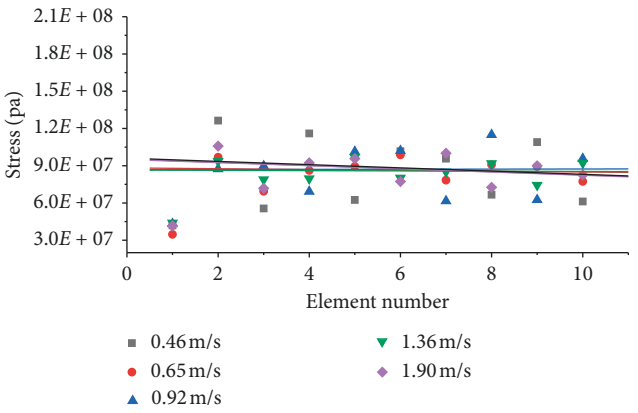

Figure 20: The average stress of representative elements under different cutting speeds ($\alpha = 10^{\circ}$ and $H = 10$ mm).

(3) The cutting depth and the back angle of the cutting tool have obvious influence on the average stress distribution of each point on the rack face. The increase of the cutting depth and the back angle could cause the maximum stress point of the rack face to move upward from the tool tip to the top, indicating that it could cause the vulnerable position of the tool to move upward along the rack face. The

cutting speed has no obvious influence on the average stress of each point on the rack face.

Data Availability

The data used to support the findings of this study are included within the article.

Conflicts of Interest

The authors declare that they have no conflicts of interest regarding the publication of this paper.

Acknowledgments

This work was supported by the National Natural Science Foundation of China (nos. 51674267 and 51874310). The support of the Yue Qi Young Scholar Project, China University of Mining & Technology, Beijing, is also acknowledged.

References

[1] D. Vogt, "A review of rock cutting for underground mining: past, present, and future," *Journal of the Southern African Institute of Mining and Metallurgy*, vol. 116, no. 11, pp. 1011–1026, 2016.

[2] G. Hammond and A. O'grady, "Indicative energy technology assessment of UK shale gas extraction," *Applied Energy*, vol. 185, pp. 1907–1918, 2017.

[3] T. P. Gouache, Y. Gao, P. Coste, and Y. Gourinat, "First experimental investigation of dual-reciprocating drilling in planetary regoliths: proposition of penetration mechanics," *Planetary and Space Science*, vol. 59, no. 13, pp. 1529–1541, 2011.

[4] B. J. Katz, "Hydrocarbon shows and source rocks in scientific ocean drilling," *International Journal of Coal Geology*, vol. 54, no. 1-2, pp. 139–154, 2003.

[5] Y. Gao, Y. Chen, Z. Wang, L. Chen, X. Zhao, and B. Sun, "Experimental study on heat transfer in hydrate-bearing reservoirs during drilling processes," *Ocean Engineering*, vol. 183, pp. 262–269, 2019.

[6] V. Prajapati, *Modeling of Rock Failure under PDC Cutter Based on Lab Experiments. Master Thesis*, Texas Technology University, Lubbock, TX, USA, 2011.

[7] Y. Nishimatsu, "The mechanics of rock cutting," *International Journal of Rock Mechanics and Mining Sciences & Geomechanics Abstracts*, vol. 9, no. 2, pp. 261–270, 1972.

[8] L. Sikarshie and J. Altiero, "The formation of chips in the penetration of elastic-brittle materials (rock)," *Transactions Journal of Apply Mechanics*, vol. 9, pp. 25–31, 1973.

[9] L. H. Chen and J. F. Labuz, "Indentation of rock by wedge-shaped tools," *International Journal of Rock Mechanics and Mining Sciences*, vol. 43, no. 7, pp. 1023–1033, 2006.

[10] Y. Zhou, W. Zhang, I. Gamwo, and J.-S. Lin, "Mechanical specific energy versus depth of cut in rock cutting and drilling," *International Journal of Rock Mechanics and Mining Sciences*, vol. 100, pp. 287–297, 2017.

[11] Q. Wang, S. Gao, S. Li et al., "Upper bound analytic mechanics model for rock cutting and its application in field testing," *Tunnelling and Underground Space Technology*, vol. 73, pp. 287–294, 2018.

[12] M. Entacher and E. Schuller, "Angular dependence of rock cutting forces due to foliation," *Tunnelling and Underground Space Technology*, vol. 71, pp. 215–222, 2018.

[13] K. Hirokazu, O. Tetsuji, M. Kuniyuki, and A. Eko, "Experimental results on the effect of bit wear on torque response," *International Journal of Rock Mechanics & Mining Sciences*, vol. 84, pp. 1–9, 2016.

[14] R. Teale, "The mechanical excavation of rock-experiments with roller cutters," *International Journal of Rock Mechanics and Mining Sciences & Geomechanics Abstracts*, vol. 1, no. 1, pp. 63–78, 1964.

[15] X. Huang, Q. Liu, L. Chen et al., "Cutting force measurement and analyses of shell cutters on a mixshield tunnelling machine," *Tunnelling and Underground Space Technology*, vol. 82, pp. 325–345, 2018.

[16] Y. Kuang, M. Zhang, M. Feng, C. Guo, and Y. Zhang, "Simulation model of PDC tooth cutting rock and experimental research on the bit," *Chinese Journal of Underground Space and Engineering*, vol. 14, pp. 1218–1225, 2018.

[17] Y. Ouyang and Q. Yang, "Numerical simulation of rock cutting in 3D with SPH method and estimation of cutting force," *Journal of Shanghai Jiao Tong University*, vol. 50, pp. 84–90, 2016.

[18] G. Li, W. Wang, Z. Jing, L. Zuo, F. Wang, and Z. Wei, "Mechanism and numerical analysis of cutting rock and soil by TBM cutting tools," *Tunnelling and Underground Space Technology*, vol. 81, pp. 428–437, 2018.

[19] C. Ji, J. Shi, Z. Liu, and Y. Wang, "Comparison of tool–chip stress distributions in nano-machining of monocrystalline silicon and copper," *International Journal of Mechanical Sciences*, vol. 77, pp. 30–39, 2013.

[20] M. Pradeep and M. R. Lovell, "Influence of rock mechanical properties and rake angle on the formation of rock fragments during cutting operation," *The International Journal of Advanced Manufacturing Technology*, vol. 90, no. 1–4, pp. 127–139, 2017.

[21] S. Yang, J. Sun, H. Li, and L. Han, "Tool failure analysis and cutting parameter optimization of coated carbides in precipitation-hardening stainless steel high feed rate milling," *China Mechanical Engineering*, vol. 27, pp. 3288–3293, 2016.

[22] X. Zhang, S. Wu, and C. Liu, "The periodical fluctuation of residual stress in hard turned surface and its relationship with chip formation," in *Proceedings of the ASME 2011 International Manufacturing Science and Engineering Conference*, Corvallis, OR, USA, June 2011.

[23] C. Ma and Z. Wang, "Experimental and numerical investigation of the breakage of a cutting tool with ultrasonic vibration," *Precision Engineering*, vol. 51, pp. 393–402, 2018.

[24] E. Detournay and C. Atkinson, "Influence of pore pressure on the drilling response in low-permeability shear-dilatant rocks," *International Journal of Rock Mechanics and Mining Sciences*, vol. 37, no. 7, pp. 1091–1101, 2000.

[25] X. H. Zhu and Y. J. Jia, "3D mechanical modeling of soil orthogonal cutting under a single reamer cutter based on Drucker–Prager criterion," *Tunnelling and Underground Space Technology*, vol. 41, pp. 255–262, 2014.

[26] C. Yang, Y. Lai, X. Wang, J. Gao, and Z. Wei, "Numerical calculation of shield cutter in sandy pebble stratum of Yellow river for Lanzhou subway," *Journal of Vibration and Shock*, vol. 37, pp. 28–33, 2018.

[27] Z. Xu, *Numerical simulation and experimental study of rock breaking mechanism by shield machine cutters*, Ph.D. thesis, Central South University, Changsha, China, 2012.

[28] Y. Yang, C. Zhang, M. Lin, and L. Chen, "Research on rock-breaking mechanism of cross-cutting PDC bit," *Journal of Petroleum Science and Engineering*, vol. 161, pp. 657–666, 2018.

[29] W. Zhang, *Finite Element Analysis of End-Milling Cutter's Cut-In Process Research and Fracture Prediction*, MS thesis, Shanghai Jiao Tong University, Shanghai, China, 2011.

[30] H. Song, H. Shi, Z. Ji et al., "The percussive process and energy transfer efficiency of percussive drilling with consideration of rock damage," *International Journal of Rock Mechanics and Mining Sciences*, vol. 119, pp. 1–12, 2019.